Non-invasive ultrasonic modulation of visual evoked response by GABA delivery through the blood brain barrier

Pierre Pouget, Charlotte Constans, Harry Ahnine, Mathieu Santin, Stéphane Lehericy, Mickael Tanter, Jean-François Aubry

Non-invasive ultrasonic modulation of visual evoked response by GABA delivery through the blood brain barrier

Authors :

1- Charlotte Constans INSERM U979 ; CNRS UMR 7587 ; Institut Langevin, Paris, France ; ESPCI Paris, PSL Research University ; Université Paris Diderot, Sorbonne Paris Cité, Paris, France
2- Harry Ahnine Institut du Cerveau et de la Moelle épinière, ICM, Centre de NeuroImagerie de Recherche, CENIR, Inserm U 1127, CNRS UMR 7225, Sorbonne Université, F-75013, Paris, France
3- Mathieu Santin Institut du Cerveau et de la Moelle épinière, ICM, Centre de NeuroImagerie de Recherche, CENIR, Inserm U 1127, CNRS UMR 7225, Sorbonne Université, F-75013, Paris, France
4- Stéphane Lehericy Institut du Cerveau et de la Moelle épinière, ICM, Centre de NeuroImagerie de Recherche, CENIR, Inserm U 1127, CNRS UMR 7225, Sorbonne Université, F-75013, Paris, France
5- Mickael Tanter INSERM U979 ; CNRS UMR 7587 ; Institut Langevin, Paris, France ; ESPCI Paris, PSL Research University ;
6- Pierre Pouget* Institut du Cerveau et de la Moelle épinière, ICM, Centre de NeuroImagerie de Recherche, CENIR, Inserm U 1127, CNRS UMR 7225, Sorbonne Université, F-75013, Paris, France
7- Jean-François Aubry* INSERM U979 ; CNRS UMR 7587 ; Institut Langevin, Paris, France ; ESPCI Paris, PSL Research University ;

* PP and JFA are co-last authors

* PP and JFA are corresponding authors: pierre.pouget@upmc.fr and jean-francois.aubry@espci.fr

Running title: GABA and BBB opening in monkeys

Keywords: Ultrasound, BBB opening, Neuromodulation, Visual Cortex, Monkey

ABSTRACT

GABA is an inhibitory neurotransmitter that is maintained outside the brain by the blood brain barrier in normal condition. In this paper we demonstrate the feasibility of modulating brain activity in the visual cortex of non-human primates by transiently permeabilizing the blood brain barrier (BBB) using focused ultrasound (FUS) coupled with ultrasound contrast agents (UCA), followed by intra-venous injection of GABA. The visual evoked potentials exhibited a significant and GABA-dose-depend decrease in activity. The effect of the sonication only (with and without UCA) was also investigated and was shown to decrease the activity 8.7 times less than the GABA-induced inhibition enabled by BBB permeabilization. Finally, the UCA harmonic response was monitored during sonication to estimate the level of stable cavitation (a signature of the effectiveness of BBB permeabilization) and to avoid damage due to inertial cavitation (the sonication was automatically shut down when this condition was detected). Our results extend the promise of the exploration and treatment of the brain using non-invasive, controllable, repeatable, and reversible neuromodulation.

INTRODUCTION

The blood brain barrier (BBB) prevents large molecules (more than 0.4 to 0.5 kDa) from diffusing through the capillary walls of the brain (Abbott & Romero 1996; Misra et al. 2003). While protecting the brain from toxic agents, it also prevents potentially therapeutic agents for brain diseases from being delivered through the blood (Aryal et al. 2014). The BBB can be temporarily and reversibly disrupted (Kroll & Neuwelt 1998; Pardridge 2005) through the intravascular injection of microbubbles coupled with low-intensity ultrasound (Hynynen et al. 2001; Hynynen et al. 2005): the acoustic wave induces bubble oscillations in the fine brain capillaries, leading to temporary permeabilization of the tight junctions between endothelial cells that ensure the BBB's effectiveness. Such BBB permeabilization lasts a few hours(Benjamin Marty et al. 2012) and its safety has been investigated in several studies on small animals (Vykhodtseva et al. 1995; McDannold et al. 2004; Liu et al. 2010; Baseri et al. 2010; Fan et al. 2017) and non-human primates (Marquet et al. 2011; McDannold et al. 2012), highlighting the possibility of effective, non-destructive BBB permeabilization in rabbits (McDannold et al. 2008) and in monkeys (McDannold et al. 2012).

The technique holds promise for therapeutic drug delivery. Pulsed ultrasound from an implanted device has been used to enhance delivery of chemotherapy to patients with glioblastoma (Carpentier et al. 2016). The technique could also provide a novel tool for non-invasive and local brain modulation by delivering inhibitory or stimulant drugs. Current neuromodulation techniques have improved dramatically in recent decades, but have certain insurmountable drawbacks: deep brain stimulation (Mayberg et al. 2005; Bronstein JM et al. 2011) and localized injection of neuroactive substances are invasive (Kringelbach et al. 2007), optogenetic methods cannot be applied to humans, and both direct current stimulation (Nitsche et al. 2009) and transcranial magnetic stimulation (Walsh & Cowey 2000; Wassermann & Lisanby 2001; Loo & Mitchell 2005) have a low spatial resolution (Chauvet et al. 2013) and are limited to cortical areas (Loo & Mitchell 2005; Brunoni et al. 2012). Interest in focused ultrasound (FUS) is increasing as a non-invasive, localized neuromodulation tool

that can be potentially applied to humans. Modulation with ultrasound alone has been demonstrated in both animals and humans. The observed effects are richly varied: modulation of EEG response(Mueller et al. 2014; Lee et al. 2016), excitation of neuronal circuits (Tyler et al. 2008; Tufail et al. 2010), modulation (Legon et al. 2014) or elicitation (Lee et al. 2015) of sensory sensations, behavioral changes (Deffieux et al. 2013; Wattiez et al. 2017), motor responses (King et al. 2013; Younan et al. 2013; Li et al. 2016; Kamimura et al. 2016; Ye et al.), suppression of somatosensory evoked potentials (SSEP) (Dallapiazza et al. 2017) and enhancement of neurogenesis (Hu et al. 2013; Scarcelli et al. 2014). However, the mechanism of FUS-induced neuromodulation is still not fully understood (Naor et al. 2016; Sassaroli & Vykhodtseva 2016) , the list of its effects is almost certainly incomplete, and studies employing it have tended to be exploratory, rather than exploiting it systematically as a tool for brain mapping or planned modulation.

The advantages of precise ultrasound focusing may be combined with the predictability of a neuroactive agent's action, should the BBB be disrupted. γ-Aminobutyric acid (GABA) is one such neuroactive agent which does not normally pass through the BBB (van Gelder & Elliott 1958). McDannold et al. (McDannold et al. 2015) temporarily suppressed the SSEP in rats by enhancing GABA delivery with ultrasonic BBB permeabilization. Zhang et al. employed magnetic-resonance guided ultrasonic BBB permeabilization to produce highly targeted lesions in rat hippocampus following the injection of a neurotoxin, quinolinic acid, which does not normally cross the blood-brain barrier (Zhang et al. 2016).

Our study is the first to show functional modulation induced by BBB permeabilization in non-human primates. We targeted the visual cortex of the animals with a single-element transducer operated at 245 kHz. We observed a decrease of the visual response intensity to full field visual stimuli and investigated the GABA dose dependency of this effect. The BBB permeabilization was confirmed twice with MRI acquisition. Moreover, we evaluated the relative impact of FUS alone, FUS with UCA, and GABA delivery on the visual response. We show that this technique is non-invasive, controllable, repeatable and reversible on

anesthetized non-human primates, with a real-time monitoring of bubble harmonic response to ensure both the safety and the effectiveness of the BBB permeabilization.

Materials and methods

Animals

Two 6-year-old captive-born macaques (Macaca mulatta 'A' and 'B'), weighing respectively 8 and 10 kg, participated to the study. Monkeys were paired-housed and handled in strict accordance with the recommendations of the Weatherall Report on good animal practice. Monkey housing conditions, surgical procedures and experimental protocols were all carried out in strict accordance with the National Institutes of Health guidelines (1996) and the recommendations of the EEC (86/609) and the French National Committee (87/848). The authorization for conducting our experiments in the institute was delivered by the Animal Health and Veterinary Medication Division of the Department of Public Veterinary Health, Nutrition and Food Safety of the French Ministry of Health (last renewal: Arrêté prefectoral N° DTPP 2010-424). Our routine laboratory procedures included an environmental enrichment program where monkeys had access to toys, mirrors and swings. Monkeys also had visual, auditory and olfactory contacts with other animals and, when appropriate, could touch/groom each other. An institutional veterinarian regularly monitored the well-being and living conditions of the monkeys.

Anesthesia was induced with a blend of ketamine hydrochloride (3 mg/kg i.m.) and dexmedetomidine (0.015 mg/kg i.m.) for initial sedation and animals were anesthetized with isoflurane during the entire procedure (1.5% during installation, 1% during experiments). After intubation, each monkey was ventilated with a mixture of isoflurane (1.5% during installation and 1% during experiments) and pure oxygen (0.5l) via a standard ventilator. Vital signs including blood oxygenation, respiration rate and end-tidal CO2 were continuously monitored. Oxygen saturation was kept at a minimum of 95% and body temperature was

maintained using a heated water blanket. An intravenous catheter was sited in the small saphenous vein to enable administration of the experimental agents. The UCA (SonoVue, Bracco, Milan, Italy) was administered in a 2ml bolus injection. 1mL contains between 100 and 500 millions of bubbles [Schneider M. Characteristics of SonoVue trade mark, Echocardiography 1999; 16(7, Pt 2):743-746]. A second injection of physiological serum with the same syringe was given a few seconds later to flush any remaining UCA.

All procedures lasted less than 3 hours. Heart rate, temperature and respiration were monitored and kept within physiological range. The animals were covered with a reflective blanket to limit the heat loss during the procedure.

Focused Ultrasound and Cavitation control

A single element FUS transducer (H117, Sonic Concept, Bothell, WA, USA) (diameter 64mm with 20mm central opening, F=1) with a passive cavitation detector (PCD) at its center (Y107, Sonic Concept, Bothell, WA, USA, 17.5mm active diameter, 64mm geometric focus, 10kHz to 20MHz bandwidth) was used at a frequency of 245 kHz. A coupling cone (C101, Sonic Concepts, Bothell, WA, USA) filled with degassed water was placed between the transducer and the animal's head. The transducer was fixed to a mechanical arm with 4 rotation axes (Viewmaster LCD, Osmond Ergonomics, Wimborne, UK) which enabled it to be flexibly positioned with respect to the head. The transducer was placed manually, targeting the middle of visual cortex V1. The tip of the cone was placed as closely parallel to the skull surface as possible. A thin layer of echographic gel (Aquasonic 100, Parker Laboratories Inc., Fairfield, NJ, USA) was applied to the shaved skin and the membrane of the coupling cone to ensure acoustic coupling.

The sonication signal (a 20ms pulse every second for 200 seconds) was created by a function generator (33250A, Agilent, Santa Clara, CA). A 75-watt amplifier (75A250A, Amplifier Research, Souderton, PA) was then used to deliver the required power to the transducer through a matching network and the input voltage of the transducer was

monitored using a voltage probe (P6139A, Tektronix, Melrose, MA) connected to an oscilloscope (Handyscope HS5, Tiepie Engineering, Sneek, The Netherlands). The amplifier gain was set to deliver a peak-to-peak output voltage (V_{out}) of 200V to the transducer. The PCD detector was directly connected to an oscilloscope (Handyscope HS5, Tiepie Engineering, Sneek, The Netherlands) with 20MS/s sampling frequency. A calibration procedure was conducted before the UCA injection. At a given amplifier gain, the amplitude of the signal generated by the first function generator was ramped up to 0.6V (in 0.02V steps), corresponding to approximately 215 V after amplification. The generator amplitude corresponding to the closest amplified voltage below 200V was chosen for the experiments. The harmonic content of the PCD recordings was then analyzed: the levels of the different harmonic types (harmonics $n*f_0$, subharmonic $f_0/2$ and ultraharmonics $(n+1/2)* f_0$) and the broadband were recorded for the selected voltage (about 200V) and used as baseline[Maimbourg, G., Houdouin, A., Santin, M., Lehericy, S., Tanter, M., & Aubry, J. F. (2018). Inside/outside the brain binary cavitation localization based on the lowpass filter effect of the skull on the harmonic content: a proof of concept study. Physics in Medicine & Biology, 63(13), 135012.].

In order to estimate the peak pressure in the brain, a clean and degassed primate skull specimen (Macaca Mulatta skull) was placed in front of the transducer in a degassed water tank and the pressure at the focus was estimated using a heterodyne interferometer (Constans et al. 2017). A heterodyne interferometer uses a laser beam to detect the vibration of a Mylar membrane induced by the ultrasound wave. The amplitude of the vibration is then converted to pressure with high sensitivity and a flat frequency response (Royer & Casula 1994).

The transmission of ultrasound through a degassed primate skull was assessed at six different points randomly chosen on the skull. The transmission was found to be 82% ± 6%. The in situ pressure delivered to the monkey brain transcranially was subsequently estimated to 0.54 ± 0.03 MPa.

Additionally, numerical simulations were performed to investigate the pressure field and amplitude inside a monkey head. The results, presented in supplementary materials (figure S2), predict a maximum amplitude pressure of 0.51 MPa, in good agreements with the previous estimations.

The equivalent mechanical index (MI) value is 1.1 with an intensity spatial peak pulse average (ISPPA) of 9.7 W/cm² in the brain. By taking into account the pulse duration and pulse repetition frequency (respectively 20ms and 1Hz, corresponding to a 2% duty cycle) during the sequence, the intensity spatial peak time average (ISPTA) is estimated to be 194mW/cm² behind the primate skull.

Visual stimuli and VEP recordings

The animals were installed in the sphinx position in front of a black screen. Their eyes were kept opened and gel (Ocry-gel, TVM, France) was applied to avoid corneal drying. The sequence of visual stimuli consisting of 200 full field white flashes separated by 2s intervals. Two electrodes were inserted symmetrically in the skin above the V1 regions. The reference electrode was subcutaneously inserted over the orbital ridge, and the ground electrode over the maxilla. The VEPs were recorded on a MAP system (Plexon Inc., TX, USA).

Sham sessions were performed without any sonication or injection of UCA or GABA, but the timing of VEP recordings was identical to a non-sham session. The transducer was positioned on the animal's head in order to reproduce the non-sham conditions but remained turned off throughout.

MRI

We ran two experiments of BBB permeabilization without the visual stimuli but with MRI assessment of Gadolinium (Gd) diffusion on monkey A. The MRCA was gadoterate meglumine (Dotarem®, Guerbet, France). We used a dose of 2mL of a 0.5mmol/mL Gd solution. The animal head was held in a stereotaxic frame during image acquisition. MRI was performed with a 3T magnet (Prisma, Siemens, Germany) using an 8-channel receive only

head coil specifically designed for non-human primate experiments (Life Services LLC, USA).

During session 1, we semi-quantitatively evaluated the signal changes due to the FUS procedure in the occipital lobe of the animal. Two-dimensional turbo spin echo T1-weighted images were acquired twice before (baseline acquisition) and after the FUS procedure and the injection of the MR contrast agent. Parameters for the T1-weighted images were: repetition time (TR) = 689 ms, echo time (TE) = 11 ms, flip angle = 90°, echo train length = 4, 8 averages, voxel size = 0.4 x 0.4 x 1.5mm^3, 10 slices, acquisition time = 7min 20sec. The signal increase was calculated as a percentage of variation between regions of interest (visual cortex, cerebellum, prefrontal cortex) and neck muscles.

During session 2, we quantitatively evaluated T1 relaxation time changes due to BBB permeabilization in the same animal. A magnetization-prepared 2 rapid gradient echo (MP2RAGE) (Marques et al. 2010) sequence was acquired twice to obtain T_1 longitudinal relaxation time parametric maps before baseline acquisition and after the FUS procedure and the injection of the MR contrast agent. Parameters for MP2RAGE were: TR = 5000ms, TE = 2.76 ms, inversion time = 700 and 2500ms, flip angle = 4° and 5°, voxel size =0.8 x 0.8 x 0.8mm^3, acquisition time = 30 min. Absolute Gd concentrations were computed to quantify the amount of delivered MR contrast agent in the target ROI using the same method as in (Benjamin Marty et al. 2012).

Data analysis

Electrophysiological data were post-processed using Matlab (MathWorks). The ground electrode signal was subtracted from the VEP recordings. The resulting signals were then filtered with a Savitzky-Golay filter (order 1, 21 ms frame length) and averaged (200 VEPs for each sequence). The offset, calculated as the mean of the first 50ms, was removed from each curve.

For the spectral power calculation, the signal was reduced to its period of interest (e.g. 0-100ms after stimulus onset) before the Fourier transform. The spectral vector was then squared and summed over its length to get the spectral power.

To standardize the analysis across all sessions, we always analyzed the first five GABA sequences, even though more data could be acquired in some sessions, with the exception of the Monkey A – 2mg/kg and Monkey B – 1 mg/kg sessions, in which we only 3 'GABA' sequences could be recorded in the time frame of the experiments.

In figure 4, the error bars represent the root mean square of the SEM of the corresponding sequences (the sequences that yielded minimum and maximum amplitudes).

In figure S5, the average harmonic response over 15 ultrasound pulses is represented on a logarithmic scale as the Fourier transform of the time signals before and after UCA injection. The plots are normalized by the resonant response at f_0 after UCA injection. Statistical analyses were performed using non-parametric ranksum *t*test ($p<0.005$) Matlab (MathWorks).

Numerical Simulations

The propagation of focused ultrasound was simulated in a monkey head to predict the pressure field in the brain (figure S2). The simulations were performed using k-Wave, a k-space pseudospectral method-based solver (Cox et al. 2007). 3D maps of the skull were extracted from a monkey CT (0.258 mm resolution, 120 kVp, Toshiba Asteion).

The transducer was modelled as a spherical section (63mm radius of curvature and 64mm active diameter). A 150 µs long pulse, spatially apodized (r=0.35) on the spherical section, was simulated at a frequency of 245 kHz. The ultrasound was propagated in water before it entered the monkey head. The simulations were first performed in pure water and compared with the amplitude measured experimentally during the calibration with a heterodyne

interferometer (Constans et al. 2017). A scaling factor was used as a correction factor in order to estimate the absolute pressure in the monkey head.

We used a linear relationship between the Hounsfield Units (HU) from the CT scan and sound speed and density. The power law model for attenuation is abs=α∗Φβ where the porosity Φ is defined by $\Phi = \frac{\rho_{max}-\rho}{\rho_{max}-\rho_{water}}$ in the skull (Aubry et al. 2003). The absorption coefficient α depends on the frequency: $\alpha = \alpha_0 f^b$.

The parameters ρ_{max}, α_0, β and b were determined in a previous work (Constans et al. 2017) by matching simulations with experimental results on a monkey skull flap.

Results

MRI

To verify the effectiveness of ultrasound-induced BBB permeabilization we performed two sessions of MRI on an anesthetized animal before and after imaging BBB permeabilization. We used 0.5mmol /mL of contrast agent (gadoterate meglumine, DOTAREM®, Guerbet, France. As the MR contrast agent (MRCA), the Dotarem has a molecular weight of 560 Da (according to the Gerbert company) and has a negative in/out GABA transport mechanisms across the BBB in healthy brain tissue (Benjamin Marty et al. 2012) . Therefore, we believe that the diffusion of MRCA into brain tissue thus indicates where the BBB has been disrupted.

During session 1, we semi-quantitatively evaluated the signal changes due to the FUS procedure in the occipital lobe of the animal. Turbo spin echo T1-weighted images were acquired twice before (baseline acquisition) and after the FUS procedure and the injection of a 2mL bolus of the contrast agent.

During session 2, we used a dedicated MRI procedure to quantitatively evaluate T1 relaxation time changes due to BBB opening in the same animal, in order to be able to

quantify the absolute gadolinium (Gd) concentration within the brain. An MP2RAGE (Marques et al. 2010) sequence was acquired twice to obtain T_1 longitudinal relaxation time parametric maps before (baseline acquisition) and after the FUS-induced BBB opening procedure.

Pre-FUS images confirmed BBB integrity before permeabilization. Signal changes in the brain tissue after the FUS procedure indicated BBB permeabilization. Both sessions yielded images showing that the BBB had been successfully disrupted on the images: after the FUS procedure, the MRCA appeared in the occipital area and to a lesser extent in the cerebellum where the ultrasound had been focused, and much less in the frontal lobes at distance from the US beam. Figure 1 displays the difference image between pre and post FUS-induced BBB permeabilization in session 1 (left) and in session 2 (right). In session 1, the signal relative to muscle increased by 75% in the visual cortex, 34% in the cerebellum, and 32% in the prefrontal cortex. In session 2, the concentration of Gadolinium was 62mM in the visual cortex, 25mM in the cerebellum and 9mM in the prefrontal cortex.

Response to visual stimuli

Figure 2 represents the timeline of the procedure. Five minutes were allowed to elapse after darkening the room before the first sequence was started (Pirenne et al. 1962). A sequence consisted of 200 successive full field white flashes, presented to the animals at intervals of 2s. Three 'baseline' sequences were performed after positioning the animal and placement of the transducer, prior to any sonication. A 'neuromodulation' sonication was then initiated, using the same ultrasound sequence as for BBB permeabilization but without injecting UCA. The VEP recording sequence entitled 'neuromodulation' was performed immediately after UCA-free sonication, 25 to 30 minutes after the beginning of the experiment. UCA injection was then performed under the low light of a flashlight, via the saphenous vein catheter. The visual stimulus with-UCA sequence was then initiated, followed by a 'BBB permeabilization,

no GABA' sequence. Finally, GABA was injected intravenously (0.1 to 6 mg/kg) and at least 3 'GABA' sequences were conducted, depending on the animal's temperature.

Figure 3 displays the VEP results from one session (monkey A, GABA dose=5 mg/kg). Each curve represents the mean of 200 responses. The 'baseline' curve corresponds to the third baseline sequence, the first two sequences being considered as a period of stabilization and dark adaptation (a total time of 20 minutes). The legend describes the sequences in chronological order. A FUS procedure without UCA is performed between the 'baseline' and 'neuromodulation' sequences. Then the BBB is disrupted with FUS and UCA injection between the 'neuromodulation' and 'No GABA' sequences. Finally, GABA was injected intravenously after the 'No GABA' sequence, and the 'GABA' sequences are conducted successively, each one lasting about 5 minutes. Sham sessions were performed without sonication or any injected agents, but the timing of VEP recordings was identical to a non-sham session, and the sequence names ('baseline', 'neuromodulation', 'no GABA', 'GABA') were maintained even though there was no neuromodulation nor GABA injection. A statistical analysis of the differences between baseline curves and GABA curves at each time point was performed. Figure S5 (supplementary materials) displays these time periods of significant difference for each session, ranked by GABA dose for both monkeys.

Figure 3: Mean VEP recordings for each sequence of stimuli from baseline to 'GABA 5' for sham sessions on both monkeys (left); GABA session: 5 mg/kg GABA dose for monkey A and 4 mg/kg for monkey B (right). Each curve represents the mean VEP recorded during one sequence of 200 stimuli. The GABA sequences are represented in orange gradient colors (red: GABA 1, yellow: GABA 5). The visual stimuli occur at time 0. Time ranges of significant differences ($p<0.005$) between baseline and neuromodulation / No GABA / GABA VEPs are indicated by the blue / dark / red horizontal lines below the curves, respectively. Figure S3 (supplementary materials) presents graphs of only 2 sequences (baseline sequence and first GABA sequence) with the standard error of the mean (SEM).

We then performed a dose study. To quantify the decrease in visual cortex activity during each session, we studied the decay of the VEP P1 amplitudes by calculating the difference between the maximum and the minimum P1 peaks over all GABA sequences. Figure 4 shows that the impact on P1 amplitude increases linearly as the GABA dose increases. To standardize the analysis across all sessions, we analyzed the first five GABA sequences, even though more data could be acquired in some sessions (in Monkey A and Monkey B, only 3 post 'GABA' sequences were recorded).

In 5 out of 7 cases, we observed significant neuromodulation effects before the GABA injection, between 100 and 300ms after the stimulus onset (figure 3 is one example). We therefore calculated the spectral power of the signals at each step: the baseline sequence, after ultrasound alone ('neuromodulation' sequence), after ultrasound coupled with UCA before GABA injection ('No GABA' sequence), and finally after GABA injection ('GABA' sequence). We calculated the mean contribution of each step in the inhibition (corresponding to the spectral power decrease) over all sessions with a GABA dose of at least 4mg/kg for three different time periods: 0-100ms, 100-200ms and 200-300ms after the stimulus onset (figure 5). The neuromodulation contribution corresponds to the decrease of activity after the 'neuromodulation' sequence, i.e. the neuromodulation spectral power minus the baseline spectral power; the UCA contribution is the decrease in activity observed after the 'no GABA' sequence, i.e. the 'No GABA' spectral power minus the neuromodulation spectral power; the GABA contribution is the decrease in activity observed during the most perturbed 'GABA' sequence. In this analysis, we considered the spectral power instead of the amplitude in order to quantify the cerebral activity at different time periods after the stimulus onset. The results showed that FUS+UCA influence increased with time after the visual stimulus onset, compared to GABA-induced effects. The percentage of GABA-induced inhibition relative to the total inhibition (combined effects of neuromodulation, UCA and GABA) is 90% during the first 100 ms, 42% during the 100-200ms period and 50% during the 200-300ms period.

UCA harmonics content

For every pulse, the signal received by the hydrophone, monitored on the second channel of the TiePie oscilloscope, was analyzed in the frequency domain. The level of broadband, harmonics, subharmonics and ultraharmonics was displayed in real time. The subharmonic is the signal at half excitation frequency $f_0/2$ (here, 245/2 = 122.5 kHz). The subharmonic emission is known to be associated with stable cavitation (Neppiras 1980; Phelps & Leighton 1997). Harmonic ($f= n*f_0$ with $n \geq 2$) and ultraharmonic ($f= (n+1/2)*f_0$ with $n \geq 1$) emissions, which are also often associated with stable cavitation (Neppiras 1980), were also recorded. The broadband emission corresponds to all the other frequencies. This noise, caused by the collapse of the bubbles, is related to inertial cavitation (Datta et al. 2006; Hwang et al. 2006).

The bolus injection took place after the beginning of ultrasound sonication, typically between the 20th and 50th seconds (out of 200). A second injection of physiological serum with the same syringe was given a few seconds later to flush any remaining UCA.

The level of the different harmonic types and the broadband were first recorded prior to UCA injection. The relative augmentation $\frac{harmoniclevel(i)-harmoniclevel(baseline)}{harmoniclevel(baseline)}$ was calculated for every ultrasonic emission #*i* for all types of harmonic and the broadband. An arbitrary safety threshold of 3 was set for the broadband maximum relative augmentation. If this value was reached, the sonication was halted automatically. An effectiveness threshold was also set to 3 for the harmonics and the subharmonic ($f_0/2$) minimum relative augmentation as an indicator of BBB permeabilization.

Discussion

Intensity of effect

After BBB permeabilization, analysis of VEPs showed a decrease of visual evoked response to full field flashes following GABA injections (figures 3, 4 and 5). Such activity was not suppressed entirely, whereas McDannold et al. (McDannold et al. 2015) almost completely

inhibited cortical primary somato-sensory (S1) activity in rats. Several hypotheses could explain this difference. Firstly, we probably did not reach the GABA dose required to completely inhibit the structures when the BBB was permeabilized. To our knowledge there is no pharmacology data on BBB permeabilization-induced GABA in the brain of primates yet, the dose was thus voluntary limited to 6 mg/kg in our study for the safety of the animals (due to the possible peripheral effects of GABA). For comparison, McDannold et al. (McDannold et al. 2015) injected up to 60mg/kg in rats. Secondly, even at a frequency as low as 245 kHz, the focal spot did not cover the entire area involved in the visual circuit, as it can be seen on the MRI (figure 1). Because of the small size of the rodent's head, BBB permeabilization was produced in both the cortex and subcortical structures such as the thalamus (McDannold et al. 2015), increasing the possibility of a complete inhibition. Thirdly, inhibiting visual cortex may not be as straightforward as inhibiting S1 cortex. The contributions of distinct primary visual areas to feedforward and feedback connections to the electrical potential recorded by VEPs are complex to disentangle. Based on peak latencies, an incremental delay between V1, V2, V3, and V3A visual latency has been reported, suggesting serial stages of processing. However, the extent to which early visual areas have distinct time courses of activation is still debated (Ales et al. 2010; Kelly et al. 2013). When direct recordings are made in monkeys, the early visual areas first become active nearly simultaneously (Schmolesky et al. 1998; Schroeder et al. 1998). Additionally, V2, V3, and V3A receive some degree of direct, subcortical input that bypasses V1 (Yoshida & Benevento 1981; Benevento & Yoshida 1981; Bullier & Kennedy 1983; Ptito et al. 1999; Sincich et al. 2004; Schmid et al. 2009).

Relative impact of GABA, BBB permeabilization and ultrasound sonication alone

Our work also estimated the relative impact of the inhibitory effects due to neuromodulation per se, without GABA. Previous studies, using a transcranial ultrasound method, McDannold et al. (McDannold et al. 2015) raised this important question of possible neuromodulation effects on the somatosensorial cortex activity during BBB permeabilization, independently of

GABA inhibition. In support to this assumption, other studies reported that ultrasound-induced neuromodulation can modulate brain function in primates (Yoo et al. 2011; Deffieux et al. 2013; Legon et al. 2014; Wattiez et al. 2017). In this study, we measured that ultrasound alone account for 1.2% of the spectral power decrease in the 0-100ms time window of the VEP recording, and for 51% in the 100-200ms time window. In comparison, BBB permeabilization alone accounts for 9% of the spectral power decrease in the 0-100ms time window of the VEP recording, and for 6% in the 100-200ms time window. Chu et al [Chu, P.-C. et al. Neuromodulation accompanying focused ultrasound-induced blood–brain barrier opening. Sci. Rep. 5, 15477; doi: 10.1038/srep15477 (2015)] also reported neuromodulation after BBB permeabilization alone. They reported a decrease of SSEP in the left primary somatosensory cortex forelimb region, elicited by right forepaw electrical stimulation when the pressure amplitude was higher than 0.35MPa. They did not observe a change of SSEP with ultrasound alone (10ms duration sonication with a 1Hz pulse repetition frequency).

Our temporally modified response of the primary visual cortex activity may indicate distinct effect of GABA inhibition and neuromodulation of ultrasound per se. Early response is a signature of the effect of GABA within V1 while later effect (>150ms) is a signature of the modulation of feedback connection. Multiple evidences support this interpretation, Firstly, single-cell recordings in non-human primates have shown that inactivation of higher-order areas modulates neuronal responses in lower-order areas (Sandell & Schiller 1982; Hupé et al. 1998; Hupé, James, Girard, & Bullier 2001; Sillito et al. 2006). It has been shown that V1 activity is modulated by GABA inhibition of area V2. Another study found similar results for V1, V2, and V3 neurons when area MT was inactivated (Hupé, James, Girard, Lomber, et al. 2001). Secondly, studies indicate feedback signals mediating surround suppression of V1 neurons. Taken together, these results strongly support the role of feedback from higher visual areas in determining V1 neural activity. Feedback interactions in human vision were also reported recently (van Kerkoerle et al. 2014). It has also have been shown that early

(40–100 ms) inactivation of V1, using transcranial magnetic stimulation (TMS), inhibits detection of simple features, but not conjunctions[56]. Finally, inactivation of V1 after longer delays (200–240 ms) seems to impair detection of feature conjunctions, while leaving simple feature detection intact. This double-dissociation implicates V1 in feedback loops with higher visual areas, although it does not specify from where such feedback might originate. Other TMS studies (Juan & Walsh 2003; Silvanto et al. 2005) specifically indicated feedback inputs from MT to V1 with latencies 80–125 ms from the stimulus onset.

Another important limitation to studies investigating the effect of GABA after BBB permeabilization is linked to the presence of influx exflux rate of large molecules via BBB transporters. In rodents, evidence has been found for the presence of a GABA-transporter in the BBB (Takanaga et al., 2001). The expression of such a transporter indicates that GABA can enter and/or exit the brain through facilitated transport. In mice, the brain efflux rate for GABA has been quantified and appears to be 17 times higher than the influx rate (Kakee et al., 2001). This complicates the interpretation of GABA concentrations in the brain, and it is possible that this may have led to an underestimation of the extent to which GABA is able to cross the BBB. That is, some studies may have found little evidence for GABA's BBB permeability because of the high efflux rate. Efflux rate in primates is unknown but the finding that GABA metabolism might differ between rodents and humans (Errante et al., 2002), no definitive conclusion are fully satisfying with regards to GABA's BBB permeability in different species yet. However, the mixed findings concerning GABA administration in clinical populations suffering from epilepsy or Huntington's disease are insufficient to rule out a possible and important effect of GABA in the brain of primates. In our experiments and we hypothesize that FUS-induced BBB disruption above the primary visual cortex enables the passage of sufficient amount of GABA to disturb functional visual responses. We speculate therefor from these results that GABA acts after entering to the brain through opened tight junctions or via intracellular transport in a quantity that overwhelms this system. As

suggested by others, it is also possible that efflux mechanisms present in the brain vasculature - the "functional" component of the BBB - are suppressed by the sonication.

Safety of ultrasound-based BBB permeabilization

Passive acoustic monitoring during BBB permeabilization has been investigated by Arvanitis et al [D. Arvanitis, M. S. Livingstone, N. Vykhodtseva, and N. McDannold,"Controlled ultrasound-induced blood-brain barrier disruption using passive acoustic emissions monitoring," PLoS ONE, vol. 7, no. 9, art. no. e45783, 2012.]. The study was performed at 220kHz, which is similar to the frequency used in our study (245kHz). Arvanitis et al did not report any damage for broadband emission with a signal to noise ratio (SNR) lower than 4.3. We measured here a mean broadband emission SNR of 1.53±0.45 and a maximum SNR of 2.20. The maximum SNR is thus lower than the threshold for safe BBB permeabilization reported by Arvanitis et al.

Conclusion:

Our study demonstrates the feasibility of modulating the activity in the visual cortex of two non-human primates by delivering GABA with transient permeabilization of the blood brain barrier using focused ultrasound coupled with ultrasound contrast agents. The effect of the sonication only (with and without UCA) was shown to be 8.7 times less than the GABA-induced inhibition. The translation of this work to the human anatomy requires further development but will be facilitated by the recent development of multi-element transcranial ultrasound devices (Lipsman et al. 2013; W. Jeff Elias et al. 2013; W. Jeffrey Elias et al. 2013; Eames et al. 2014; Marsac et al. 2017). A lower cost approach that exploits an acoustic lens which compensates for the aberrations induced by the human skull may also prove valuable (Maimbourg et al. 2018) and [Maimbourg, G., Houdouin, A., Deffieux, T., Tanter, M., & Aubry, J. F. (2019). Steering capabilities of an acoustic lens for transcranial therapy: numerical and experimental studies. IEEE Transactions on Biomedical Engineering].

Conflicts of interest

The authors of the submitted manuscript certify that they have no affiliations with or involvement in any organization or entity with any financial interest in the subject matter or materials discussed in this manuscript.

Acknowledgements

We thank Sophie Rivaud-Péchoux for her help with the statistical analysis. This work was supported by the Bettencourt Schueller Foundation, LABEX WIFI (Laboratory of Excellence within the French Program 'Investments for the Future', references ANR-10-LABX-24 and ANR-10-IDEX-0001-02 PSL), the 'future investments' program of the National Agency for Research (references ANR-10-EQPX-15, IHU-A-ICM), the Paris Institute of Translational Neuroscience (IAIHU-06), France Life Imaging (ANR-11-INBS-0006), and NeurATRIS (translational research infrastructure for biotherapies in neuroscience, reference ANR-11-INBS-0011).

REFERENCES

Abbott NJ, Romero IA. 1996. Transporting therapeutics across the blood-brain barrier. Mol Med Today. 2:106–113.

Ales JM, Yates JL, Norcia AM. 2010. V1 is not uniquely identified by polarity reversals of responses to upper and lower visual field stimuli. NeuroImage. 52:1401–1409.

Aryal M, Arvanitis CD, Alexander PM, McDannold N. 2014. Ultrasound-mediated blood–brain barrier disruptlion for targeted drug delivery in the central nervous system. Adv Drug Deliv Rev. 72:94–109.

Aubry J-F, Tanter M, Pernot M, Thomas J-L, Fink M. 2003. Experimental demonstration of noninvasive transskull adaptive focusing based on prior computed tomography scans. J Acoust Soc Am. 113:84–93.

Baseri B, Choi JJ, Tung Y-S, Konofagou EE. 2010. Multi-Modality Safety Assessment of Blood-Brain Barrier Opening Using Focused Ultrasound and Definity Microbubbles: A Short-Term Study. Ultrasound Med Biol. 36:1445–1459.

Benevento LA, Yoshida K. 1981. The afferent and efferent organization of the lateral geniculo-prestriate pathways in the macaque monkey. J Comp Neurol. 203:455–474.

Benjamin Marty, Benoit Larrat, Maxime Van Landeghem, Caroline Robic, Philippe Robert, Marc Port, Denis Le Bihan, Mathieu Pernot, Mickael Tanter, Franck Lethimonnier, Sébastien Mériaux. 2012. Dynamic Study of Blood–Brain Barrier Closure after its disruptlion using Ultrasound: A Quantitative Analysis. J Cereb Blood Flow Metab. 32:1948–1958.

Bronstein JM, Tagliati M, Alterman RL, et al. 2011. Deep brain stimulation for parkinson disease: An expert consensus and review of key issues. Arch Neurol. 68:165–165.

Brunoni AR, Nitsche MA, Bolognini N, Bikson M, Wagner T, Merabet L, Edwards DJ, Valero-Cabre A, Rotenberg A, Pascual-Leone A, et al. 2012. Clinical research with transcranial direct current stimulation (tDCS): Challenges and future directions. Brain Stimulat. 5:175–195.

Bullier J, Kennedy H. 1983. Projection of the lateral geniculate nucleus onto cortical area V2 in the macaque monkey. Exp Brain Res. 53:168–172.

Carpentier A, Canney M, Vignot A, Reina V, Beccaria K, Horodyckid C, Karachi C, Leclercq D, Lafon C, Chapelon J-Y, et al. 2016. Clinical trial of blood-brain barrier disruptlion by pulsed ultrasound. Sci Transl Med. 8:343re2-343re2.

Chauvet D, Marsac L, Pernot M, Boch A-L, Guillevin R, Salameh N, Souris L, Darrasse L, Fink M, Tanter M, Aubry J-F. 2013. Targeting accuracy of transcranial magnetic resonance–guided high-intensity focused ultrasound brain therapy: a fresh cadaver model. J Neurosurg. 118:1046–1052.

Constans C, Deffieux T, Pouget P, Tanter M, Aubry JF. 2017. A 200 - 1380 kHz Quadrifrequency Focused Ultrasound Transducer For Neurostimulation In Rodents And Primates: Transcranial In Vitro Calibration And Numerical Study Of The Influence Of Skull Cavity. IEEE Trans Ultrason Ferroelectr Freq Control. PP:1–1.

Cox BT, Kara S, Arridge SR, Beard PC. 2007. k-space propagation models for acoustically heterogeneous media: Application to biomedical photoacoustics. J Acoust Soc Am. 121:3453–3464.

Dallapiazza RF, Timbie KF, Holmberg S, Gatesman J, Lopes MB, Price RJ, Miller GW, Elias WJ. 2017. Noninvasive neuromodulation and thalamic mapping with low-intensity focused ultrasound. J Neurosurg.:1–10.

Datta S, Coussios C-C, McAdory LE, Tan J, Porter T, Courten-Myers GD, Holland CK. 2006. Correlation of cavitation with ultrasound enhancement of thrombolysis. Ultrasound Med Biol. 32:1257–1267.

Deffieux T, Younan Y, Wattiez N, Tanter M, Pouget P, Aubry J-F. 2013. Low-Intensity Focused Ultrasound Modulates Monkey Visuomotor Behavior. Curr Biol. 23:2430–2433.

Eames MD, Hananel A, Snell JW, Kassell NF, Aubry J-F. 2014. Trans-cranial focused ultrasound without hair shaving: feasibility study in an ex vivo cadaver model. J Ther Ultrasound. 1:24.

Elias W. Jeffrey, Huss D, Voss T, Loomba J, Khaled M, Zadicario E, Frysinger RC, Sperling SA, Wylie S, Monteith SJ, et al. 2013. A Pilot Study of Focused Ultrasound Thalamotomy for Essential Tremor. http://dx.doi.org/101056/NEJMoa1300962 [Internet]. [cited 2016 May 24]. Available from: http://www.nejm.org/doi/full/10.1056/NEJMoa1300962

Elias W. Jeff, Khaled M, Hilliard JD, Aubry J-F, Frysinger RC, Sheehan JP, Wintermark M, Lopes MB. 2013. A magnetic resonance imaging, histological, and dose modeling comparison of focused ultrasound, radiofrequency, and Gamma Knife radiosurgery lesions in swine thalamus. J Neurosurg. 119:307–317.

Fan C-H, Lin C-Y, Liu H-L, Yeh C-K. 2017. Ultrasound targeted CNS gene delivery for Parkinson's disease treatment. J Controlled Release. 261:246–262.

van Gelder NM, Elliott K a. C. 1958. DISPOSITION OF γ-AMINOBUTYRIC ACID ADMINISTERED TO MAMMALS*. J Neurochem. 3:139–143.

Hu Y, Zhong W, Wan JMF, Yu ACH. 2013. Ultrasound can Modulate Neuronal Development: Impact on Neurite Growth and Cell Body Morphology. Ultrasound Med Biol. 39:915–925.

Hupé JM, James AC, Girard P, Bullier J. 2001. Response modulations by static texture surround in area V1 of the macaque monkey do not depend on feedback connections from V2. J Neurophysiol. 85:146–163.

Hupé JM, James AC, Girard P, Lomber SG, Payne BR, Bullier J. 2001. Feedback connections act on the early part of the responses in monkey visual cortex. J Neurophysiol. 85:134–145.

Hupé JM, James AC, Payne BR, Lomber SG, Girard P, Bullier J. 1998. Cortical feedback improves discrimination between figure and background by V1, V2 and V3 neurons. Nature. 394:784–787.

Hwang JH, Tu J, Brayman AA, Matula TJ, Crum LA. 2006. Correlation between inertial cavitation dose and endothelial cell damage in vivo. Ultrasound Med Biol. 32:1611–1619.

Hynynen K, McDannold N, Sheikov NA, Jolesz FA, Vykhodtseva N. 2005. Local and reversible blood–brain barrier disruption by noninvasive focused ultrasound at frequencies suitable for trans-skull sonications. NeuroImage. 24:12–20.

Hynynen K, McDannold N, Vykhodtseva N, Jolesz FA. 2001. Noninvasive MR Imaging–guided Focal Opening of the Blood-Brain Barrier in Rabbits. Radiology. 220:640–646.

Juan C-H, Walsh V. 2003. Feedback to V1: a reverse hierarchy in vision. Exp Brain Res. 150:259–263.

Kamimura HAS, Wang S, Chen H, Wang Q, Aurup C, Acosta C, Carneiro AAO, Konofagou EE. 2016. Focused ultrasound neuromodulation of cortical and subcortical brain structures using 1.9 MHz: FUS neuromodulation of cortical/subcortical brain structures. Med Phys. 43:5730–5735.

Kelly SP, Schroeder CE, Lalor EC. 2013. What does polarity inversion of extrastriate activity tell us about striate contributions to the early VEP? A comment on Ales et al. (2010). NeuroImage. 76:442–445.

van Kerkoerle T, Self MW, Dagnino B, Gariel-Mathis M-A, Poort J, van der Togt C, Roelfsema PR. 2014. Alpha and gamma oscillations characterize feedback and feedforward processing in monkey visual cortex. Proc Natl Acad Sci. 111:14332–14341.

King RL, Brown JR, Newsome WT, Pauly KB. 2013. Effective Parameters for Ultrasound-Induced In Vivo Neurostimulation. Ultrasound Med Biol. 39:312–331.

Kringelbach ML, Jenkinson N, Owen SLF, Aziz TZ. 2007. Translational principles of deep brain stimulation. Nat Rev Neurosci. 8:623–635.

Kroll RA, Neuwelt EA. 1998. Outwitting the blood-brain barrier for therapeutic purposes: osmotic opening and other means. Neurosurgery. 42:1083–1099; discussion 1099-1100.

Lee W, Kim H, Jung Y, Song I-U, Chung YA, Yoo S-S. 2015. Image-Guided Transcranial Focused Ultrasound Stimulates Human Primary Somatosensory Cortex. Sci Rep. 5:8743.

Lee W, Lee SD, Park MY, Foley L, Purcell-Estabrook E, Kim H, Fischer K, Maeng L-S, Yoo S-S. 2016. Image-Guided Focused Ultrasound-Mediated Regional Brain Stimulation in Sheep. Ultrasound Med Biol. 42:459–470.

Legon W, Sato TF, Opitz A, Mueller J, Barbour A, Williams A, Tyler WJ. 2014. Transcranial focused ultrasound modulates the activity of primary somatosensory cortex in humans. Nat Neurosci. 17:322–329.

Li G-F, Zhao H-X, Zhou H, Yan F, Wang J-Y, Xu C-X, Wang C-Z, Niu L-L, Meng L, Wu S, et al. 2016. Improved Anatomical Specificity of Non-invasive Neuro-stimulation by High Frequency (5 MHz) Ultrasound. Sci Rep. 6:24738.

Lipsman N, Schwartz ML, Huang Y, Lee L, Sankar T, Chapman M, Hynynen K, Lozano AM. 2013. MR-guided focused ultrasound thalamotomy for essential tremor: a proof-of-concept study. Lancet Neurol. 12:462–468.

Liu H-L, Hua M-Y, Yang H-W, Huang C-Y, Chu P-C, Wu J-S, Tseng I-C, Wang J-J, Yen T-C, Chen P-Y, Wei K-C. 2010. Magnetic resonance monitoring of focused ultrasound/magnetic nanoparticle targeting delivery of therapeutic agents to the brain. Proc Natl Acad Sci. 107:15205–15210.

Loo CK, Mitchell PB. 2005. A review of the efficacy of transcranial magnetic stimulation (TMS) treatment for depression, and current and future strategies to optimize efficacy. J Affect Disord. 88:255–267.

Maimbourg G, Houdouin A, Deffieux T, Tanter M, Aubry J-F. 2018. 3D-printed adaptive acoustic lens as a disruptive technology for transcranial ultrasound therapy using single-element transducers. Phys Med Biol. 63:025026.

Marques JP, Kober T, Krueger G, van der Zwaag W, Van de Moortele P-F, Gruetter R. 2010. MP2RAGE, a self bias-field corrected sequence for improved segmentation and T1-mapping at high field. NeuroImage. 49:1271–1281.

Marquet F, Tung Y-S, Teichert T, Ferrera VP, Konofagou EE. 2011. Noninvasive, Transient and Selective Blood-Brain Barrier Opening in Non-Human Primates In Vivo. PLOS ONE. 6:e22598.

Marsac L, Chauvet D, Greca RL, Boch A-L, Chaumoitre K, Tanter M, Aubry J-F. 2017. Ex vivo optimisation of a heterogeneous speed of sound model of the human skull for

non-invasive transcranial focused ultrasound at 1 MHz. Int J Hyperthermia. 33:635–645.

Mayberg HS, Lozano AM, Voon V, McNeely HE, Seminowicz D, Hamani C, Schwalb JM, Kennedy SH. 2005. Deep Brain Stimulation for Treatment-Resistant Depression. Neuron. 45:651–660.

McDannold N, Arvanitis CD, Vykhodtseva N, Livingstone MS. 2012. Temporary Disruption of the Blood–Brain Barrier by Use of Ultrasound and Microbubbles: Safety and Efficacy Evaluation in Rhesus Macaques. Cancer Res. 72:3652–3663.

McDannold N, Vykhodtseva N, Hynynen K. 2008. Blood-Brain Barrier Disruption Induced by Focused Ultrasound and Circulating Preformed Microbubbles Appears to Be Characterized by the Mechanical Index. Ultrasound Med Biol. 34:834–840.

McDannold N, Vykhodtseva N, Jolesz FA, Hynynen K. 2004. MRI investigation of the threshold for thermally induced blood-brain barrier disruption and brain tissue damage in the rabbit brain. Magn Reson Med. 51:913–923.

McDannold N, Zhang Y, Power C, Arvanitis CD, Vykhodtseva N, Livingstone M. 2015. Targeted, noninvasive blockade of cortical neuronal activity. Sci Rep [Internet]. 5. Available from: https://www.ncbi.nlm.nih.gov/pmc/articles/PMC4635366/

Misra A, Ganesh S, Shahiwala A, Shah SP. 2003. Drug delivery to the central nervous system: a review. J Pharm Pharm Sci Publ Can Soc Pharm Sci Soc Can Sci Pharm. 6:252–273.

Mueller J, Legon W, Opitz A, Sato TF, Tyler WJ. 2014. Transcranial Focused Ultrasound Modulates Intrinsic and Evoked EEG Dynamics. Brain Stimul Basic Transl Clin Res Neuromodulation. 7:900–908.

Naor O, Krupa S, Shoham S. 2016. Ultrasonic neuromodulation. J Neural Eng. 13:031003.

Neppiras EA. 1980. Acoustic cavitation. Phys Rep. 61:159–251.

Nitsche MA, Boggio PS, Fregni F, Pascual-Leone A. 2009. Treatment of depression with transcranial direct current stimulation (tDCS): A Review. Exp Neurol. 219:14–19.

Pardridge WM. 2005. The Blood-Brain Barrier: Bottleneck in Brain Drug Development. NeuroRX. 2:3–14. After a first rapid adaptation of the cones (5 to 8 minutes), a second mechanism of vision comes into play, where there is another decrease in threshold with a slower decline. The curve asymptotes to a minimum (absolute threshold) at about 10-5 cd/m2after about twenty minutes in the dark.

Pirenne M. H., Dark Adaptation and Night Vision. In: Davson, H. (ed), The Eye, vol 2. London, Academic Press, 1962

Phelps AD, Leighton TG. 1997. The Subharmonic Oscillations And Combination-Frequency Subharmonic Emissions From A Resonant Bubble: Their Properties and Generation Mechanisms. Acta Acust United Acust. 83:59–66.

Ptito M, Johannsen P, Faubert J, Gjedde A. 1999. Activation of human extrageniculostriate pathways after damage to area V1. NeuroImage. 9:97–107.

Royer D, Casula O. 1994. Quantitative imaging of transient acoustic fields by optical heterodyne interferometry. In: 1994 IEEE Ultrason Symp 1994 Proc. Vol. 2. [place unknown]; p. 1153–1162 vol.2.

Sandell JH, Schiller PH. 1982. Effect of cooling area 18 on striate cortex cells in the squirrel monkey. J Neurophysiol. 48:38–48.

Sassaroli E, Vykhodtseva N. 2016. Acoustic neuromodulation from a basic science prospective. J Ther Ultrasound. 4:17.

Scarcelli T, Jordão JF, O'Reilly MA, Ellens N, Hynynen K, Aubert I. 2014. Stimulation of Hippocampal Neurogenesis by Transcranial Focused Ultrasound and Microbubbles in Adult Mice. Brain Stimulat. 7:304–307.

Schmid MC, Panagiotaropoulos T, Augath MA, Logothetis NK, Smirnakis SM. 2009. Visually driven activation in macaque areas V2 and V3 without input from the primary visual cortex. PloS One. 4:e5527.

Schmolesky MT, Wang Y, Hanes DP, Thompson KG, Leutgeb S, Schall JD, Leventhal AG. 1998. Signal timing across the macaque visual system. J Neurophysiol. 79:3272–3278.

Schroeder CE, Mehta AD, Givre SJ. 1998. A spatiotemporal profile of visual system activation revealed by current source density analysis in the awake macaque. Cereb Cortex N Y N 1991. 8:575–592.

Sillito AM, Cudeiro J, Jones HE. 2006. Always returning: feedback and sensory processing in visual cortex and thalamus. Trends Neurosci. 29:307–316.

Silvanto J, Lavie N, Walsh V. 2005. Double dissociation of V1 and V5/MT activity in visual awareness. Cereb Cortex N Y N 1991. 15:1736–1741.

Sincich LC, Park KF, Wohlgemuth MJ, Horton JC. 2004. Bypassing V1: a direct geniculate input to area MT. Nat Neurosci. 7:1123–1128.

Tufail Y, Matyushov A, Baldwin N, Tauchmann ML, Georges J, Yoshihiro A, Tillery SIH, Tyler WJ. 2010. Transcranial Pulsed Ultrasound Stimulates Intact Brain Circuits. Neuron. 66:681–694.

Tyler WJ, Tufail Y, Finsterwald M, Tauchmann ML, Olson EJ, Majestic C. 2008. Remote Excitation of Neuronal Circuits Using Low-Intensity, Low-Frequency Ultrasound. PLOS ONE. 3:e3511.

Vykhodtseva NI, Hynynen K, Damianou C. 1995. Histologic effects of high intensity pulsed ultrasound exposure with subharmonic emission in rabbit brain in vivo. Ultrasound Med Biol. 21:969–979.

Walsh V, Cowey A. 2000. Transcranial magnetic stimulation and cognitive neuroscience. Nat Rev Neurosci. 1:73–80.

Wassermann EM, Lisanby SH. 2001. Therapeutic application of repetitive transcranial magnetic stimulation: a review. Clin Neurophysiol. 112:1367–1377.

Wattiez N, Constans C, Deffieux T, Daye PM, Tanter M, Aubry J-F, Pouget P. 2017. Transcranial ultrasonic stimulation modulates single-neuron discharge in macaques performing an antisaccade task. Brain Stimulat [Internet]. Available from: http://www.sciencedirect.com/science/article/pii/S1935861X17308471

Ye PP, Brown JR, Pauly KB. Frequency Dependence of Ultrasound Neurostimulation in the Mouse Brain. Ultrasound Med Biol [Internet]. [cited 2016 May 25]. Available from: http://www.sciencedirect.com/science/article/pii/S0301562916001046

Yoo S-S, Bystritsky A, Lee J-H, Zhang Y, Fischer K, Min B-K, McDannold NJ, Pascual-Leone A, Jolesz FA. 2011. Focused ultrasound modulates region-specific brain activity. NeuroImage. 56:1267–1275.

Yoshida K, Benevento LA. 1981. The projection from the dorsal lateral geniculate nucleus of the thalamus to extrastriate visual association cortex in the macaque monkey. Neurosci Lett. 22:103–108.

Younan Y, Deffieux T, Larrat B, Fink M, Tanter M, Aubry J-F. 2013. Influence of the pressure field distribution in transcranial ultrasonic neurostimulation. Med Phys. 40:082902.

Zhang Y, Tan H, Bertram EH, Aubry J-F, Lopes M-B, Roy J, Dumont E, Xie M, Zuo Z, Klibanov AL, et al. 2016. Non-Invasive, Focal Disconnection of Brain Circuitry Using

Magnetic Resonance-Guided Low-Intensity Focused Ultrasound to Deliver a Neurotoxin. Ultrasound Med Biol. 42:2261–2269.

CAPTION FIGURES:

Figure 1: MRI assessment of BBB disruption. Difference images between pre and post FUS-induced BBB disruption in session 1 (left) and in session 2 (right). Three ROIs outline the visual cortex (red), the cerebellum (green) and the prefrontal reference (blue). The orange ellipses representing the ultrasound focal area based on numerical simulations are shown in figure S3. V1 was manually segmented on the T1-weighted MP-RAGE images. The blood brain barrier opening zone was also manually segmented on the T1-weighted spin-echo images after Dotarem injection based on the hyperintense signal. The two ROIs were then registered using spm12(http://store.elsevier.com/product.jsp?isbn=9780123725608). ROIs overlap was then computed to estimate the percentage of blood barrier in primary visual cortex that was considered as opened. Our quantification reveals that 12% of the primary cortex (including V1, V2 and V3) estimated by Dotarem extravasation.

Figure 2: a) Experimental set-up. A 0.1s-long full field white flash appears every 2s in front of the anesthetized animal. b) Timeline of the BBB disruption experiments. Each vertical bar represents a VEP sequence, measuring the visual responses to 200 full field flashes. 3 baseline sequences are first conducted (t=5-20 min). FUS (focused ultrasound) sonication is then performed without UCA (ultrasound contrast agent) injection before the 'Neuromodulation' sequence at t=25-30 min. The BBB is then disrupted with the FUS + UCA injection. The 'No GABA' sequence then occurs at t=40-45min. Finally, GABA is injected and at least three 'GABA' sequences are conducted. c) Timeline of the sham experiments. The timing is identical to a BBB disruption session, but no sonication or injections are administered.

Figure 3: Mean VEP recordings for each sequence of stimuli from baseline to 'GABA 5' for sham sessions on both monkeys (left); GABA session: 5 mg/kg GABA dose for monkey A and 4 mg/kg for monkey B (right). Each curve represents the mean VEP recorded during one sequence of 200 stimuli. The GABA sequences are represented in orange gradient colors (red: GABA 1, yellow: GABA 5). The visual stimuli occur at time 0. Time ranges of significant differences ($p<0.005$) between baseline and neuromodulation / No GABA / GABA VEPs are indicated by the blue / dark / red horizontal lines below the curves, respectively. Figure S4 (supplementary materials) presents graphs of only 2 sequences (baseline sequence and first GABA sequence) with the standard error of the mean (SEM).

Figure 4: Decrease in VEP amplitude (maximum P1 amplitude – minimum P1 amplitude over the five first GABA sequences (except for monkey A - 2mg and monkey B - 1mg with only 3 GABA sequences, in light colors) after GABA injection, as a function of GABA dose.

Figure 5: Proportion of the inhibitory effects due to neuromodulation (ultrasound only), BBB disruption (ultrasound + UCA) and GABA (after BBB disruption and GABA injection). Top: Illustration of the calculation of the contributions from the three events for one session (monkey A, GABA: 5 mg/kg). Bottom: Quantification (average of all sessions with a GABA dose of at least 4mg/kg in monkey A and monkey B) of the contributions from neuromodulation, UCA and GABA on VEP spectral power decrease, for three different time periods. Above each time period, the inset displays

the normalized mean spectral power of baseline VEPs (dark green), post FUS or neuromodulation VEPs (green), post FUS+UCA VEPs (light green) and GABA VEPs (red).

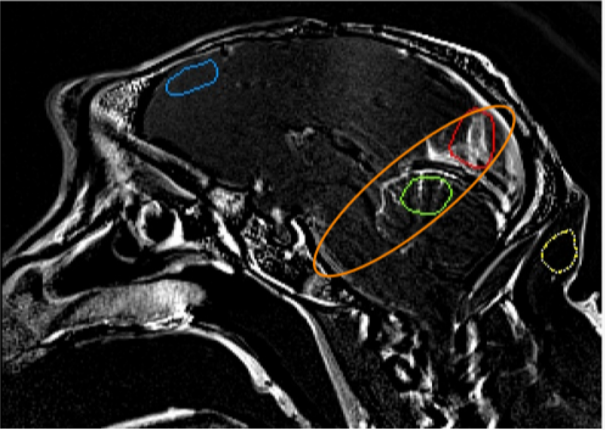
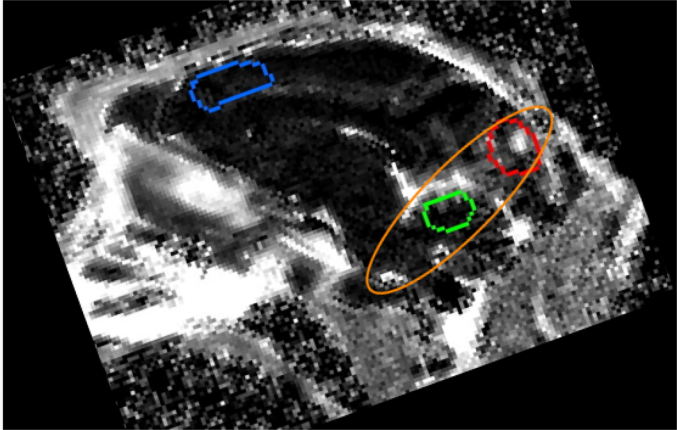

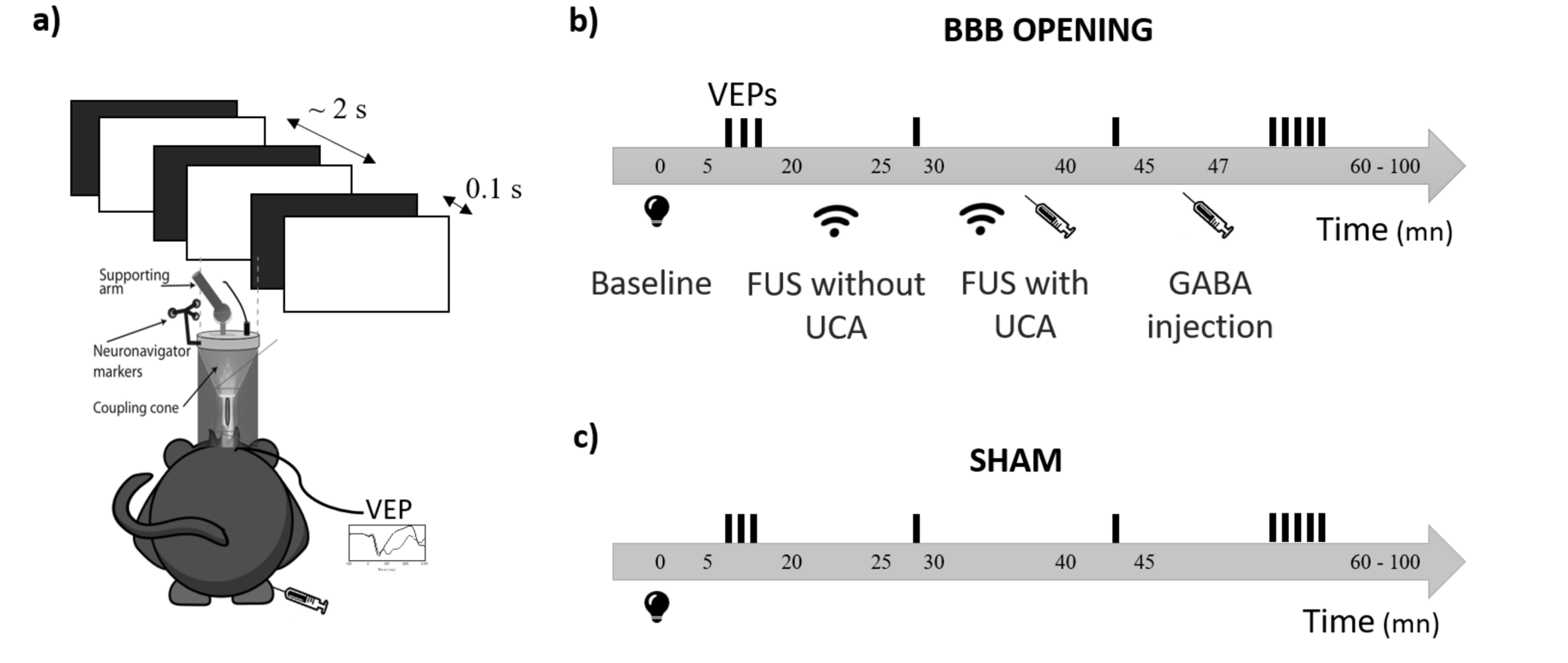
a)
~ 2 s
0.1 s
Supporting arm
Neuronavigator markers
Coupling cone
VEP
b)
BBB OPENING
VEPs
0
5
20
25
30
40
45
47
60 - 100
Time (mn)
Baseline
FUS without UCA
FUS with UCA
GABA injection
c)
SHAM
0
5
20
25
30
40
45
60 - 100
Time (mn)

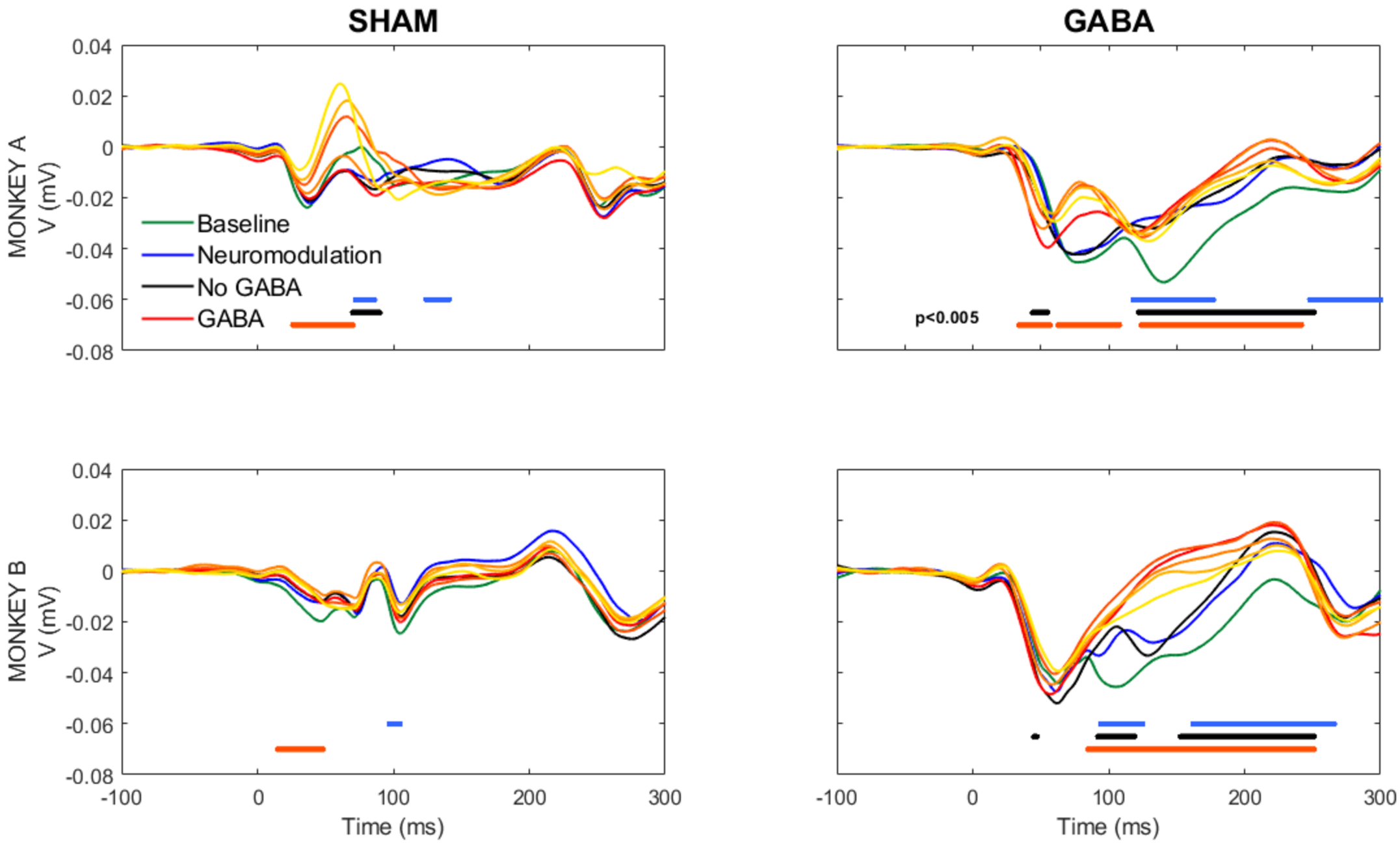
SHAM
GABA
MONKEY A
MONKEY B
V (mV)
0.04
0.02
0
-0.02
-0.04
-0.06
-0.08
Baseline
Neuromodulation
No GABA
GABA
p<0.005
-100
0
100
200
300
Time (ms)

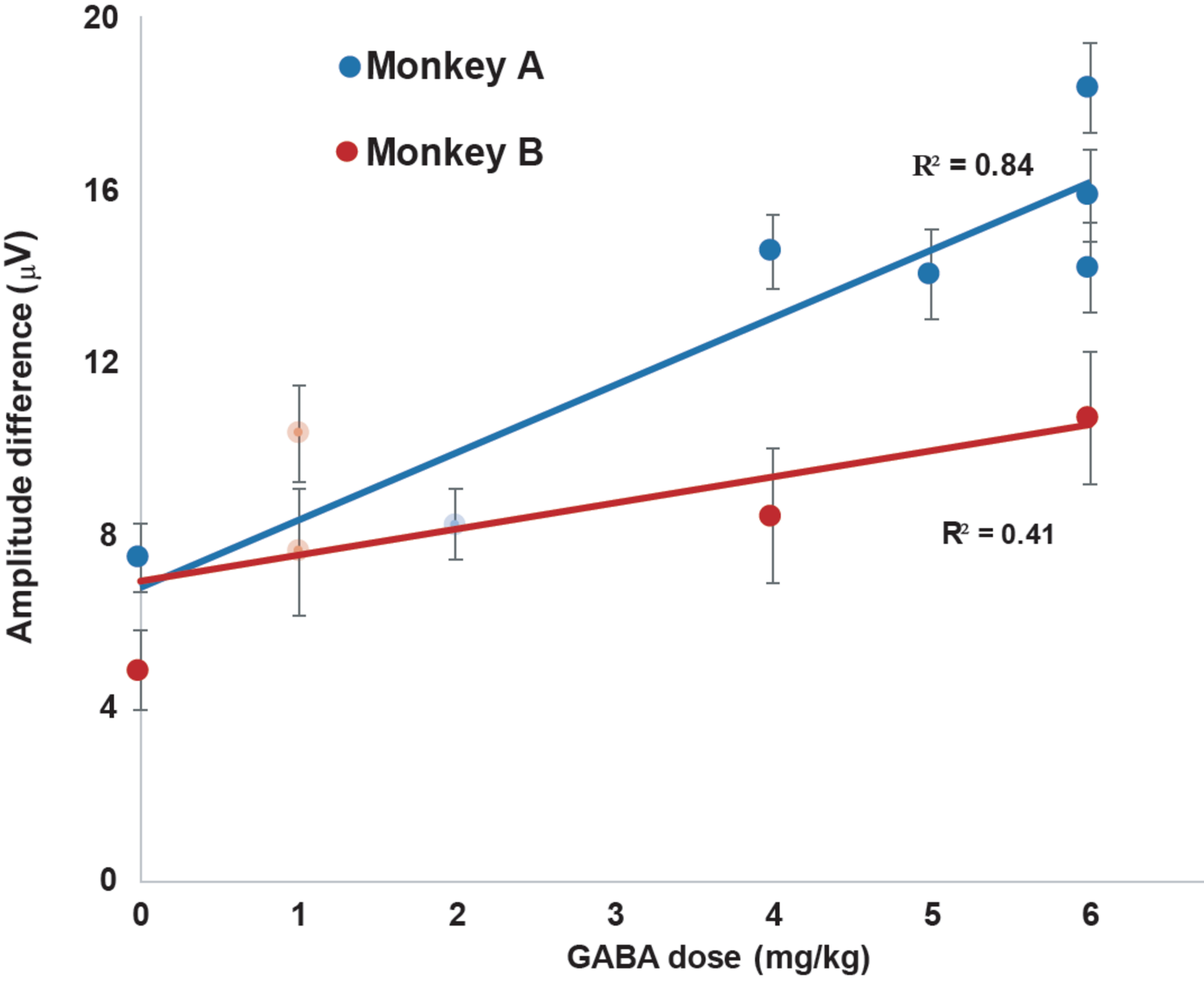
Monkey A
Monkey B
R² = 0.84
R² = 0.41
Amplitude difference (μV)
GABA dose (mg/kg)
0
4
8
12
16
20
0
1
2
3
4
5
6

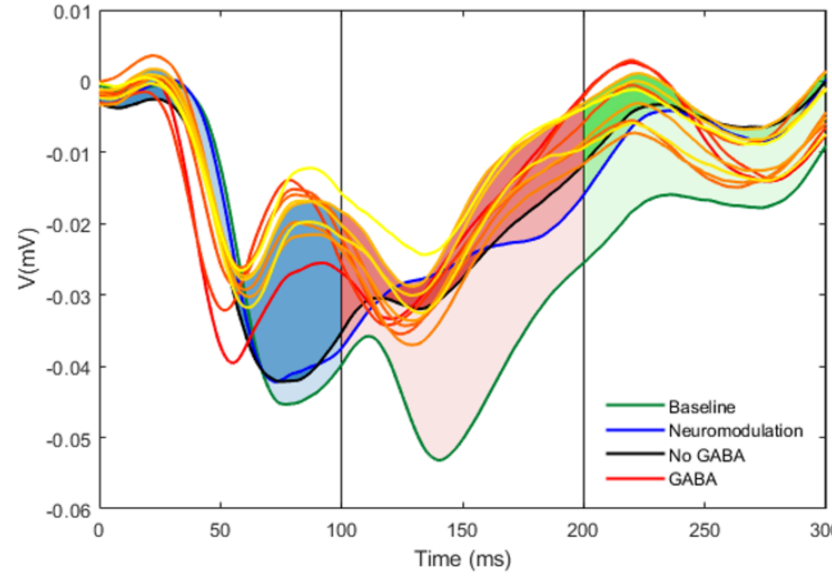
0.01
0
-0.01
-0.02
-0.03
-0.04
-0.05
-0.06
V(mV)
0
50
100
150
200
250
300
Time (ms)
Baseline
Neuromodulation
No GABA
GABA

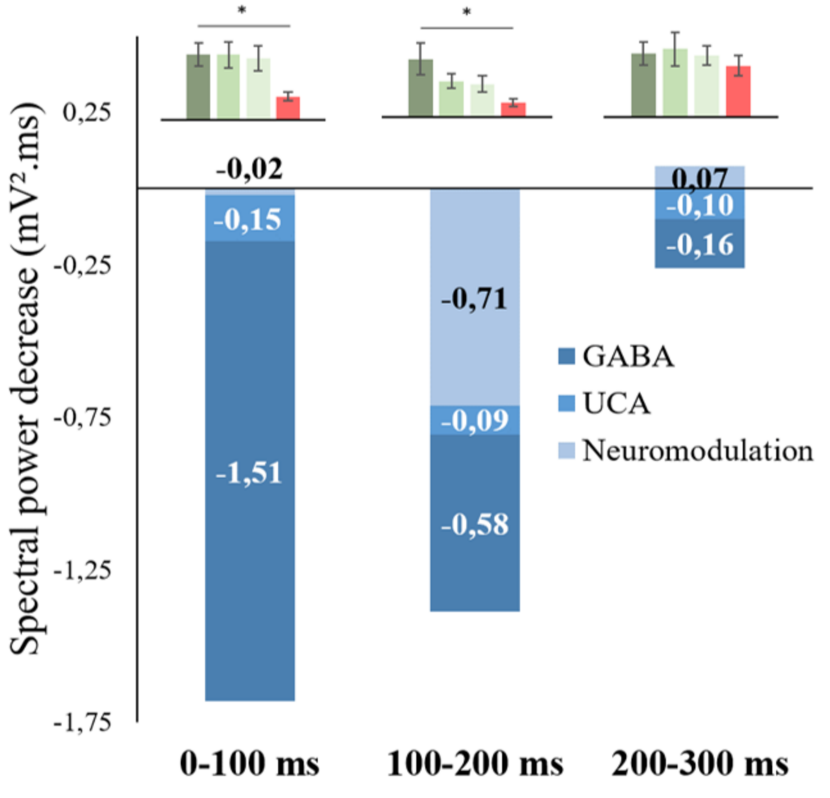
*
*
0,25
-0,25
-0,75
-1,25
-1,75
Spectral power decrease (mV².ms)
-0,02
-0,15
-1,51
-0,71
-0,09
-0,58
0,07
-0,10
-0,16
GABA
UCA
Neuromodulation
0-100 ms
100-200 ms
200-300 ms

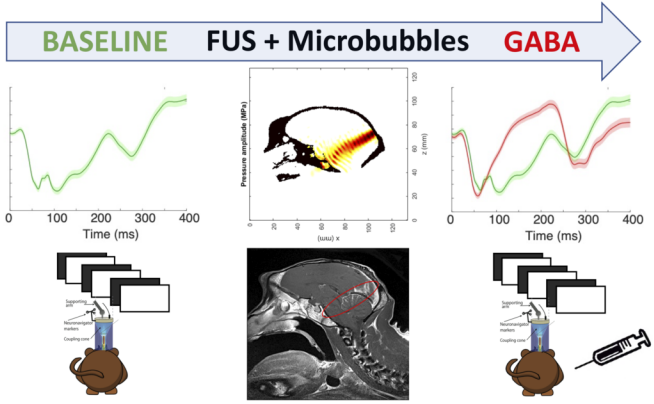
BASELINE
FUS + Microbubbles
GABA
0
100
200
300
400
Time (ms)
Pressure amplitude (MPa)
z (mm)
(uuu) x
Supporting arm
Neuronavigation markers
Coupling cone